J. Iron Steel Res. Int. (2021) 28:1233–1242
https://doi.org/10.1007/s42243-021-00635-w

ORIGINAL PAPER

Properties of ten-year-aged argon oxygen decarburization stainless steel slag

Ya-jun Wang[1,2] · Ya-nan Zeng[1] · Jun-guo Li[1] · Yu-zhu Zhang[1,2] · Wei Wang[1]

Received: 25 August 2020 / Revised: 16 November 2020 / Accepted: 18 November 2020 / Published online: 25 August 2021

Abstract
The characteristics of argon oxygen decarburization slag (AODS) for smelting stainless steel that has been aged for 10 years were analyzed. Three types of AODSs distributed at three positions in a slag heap were sampled for comparison experiments. Chemical analysis, mineral phase identification, thermogravimetric analysis, and micromorphology analysis were used to study the element migration trends and carbonation behavior of AODS after long-term aging. Sequential leaching tests were performed to study the chromium leachability of the aged AODS. The results show that during the long-term aging process, the AODS heap had undergone oxidation and carbonation, accompanied by element migration and mineralogical evolution. The surface slag had the highest degree of carbonation but the weakest chromium leachability. The chemical composition of the middle slag was the closest to that of the original slag. In the bottom steel slag, in addition to magnesium, certain depositions of other elements were present. The matrix phases in the aged slag were dicalcium silicate and merwinite, and the chromium was mainly wrapped in these matrix phases in the form of oxides, spinels, or alloys. Under the combined effects of carbonation and oxidation, the leaching characteristics of the chromium in the aged slag varied greatly depending on the location. The bottom slag had the strongest chromium leachability, and the hexavalent chromium had long-term continuous leachability.

Keywords Argon oxygen decarburization slag · Aging · Chromium · Leaching · Mineral phase

1 Introduction

In 2019, China produced 29.4 million tons of crude stainless steel [1], accompanied by more than 9.0 million tons of stainless steel slag [2]. Three kinds of stainless steel slags are produced in the three processes of smelting stainless steel, namely, electric arc furnace slag (EAFS), argon oxygen decarburization slag (AODS) and ladle metallurgy slag (LMS) [3].

AODS is a by-product generated in the AOD (argon oxygen decarburization) furnace during the refining step of the stainless steel smelting process. AODS has high contents of CaO, SiO_2, and MgO, as well as some Cr_2O_3 and fluorine [4]. In its cold state, the crystalline mineral phase composition of AODS mainly includes γ-dicalcium silicate (γ-$2CaO{\cdot}SiO_2$ (γ-C_2S)), β-dicalcium silicate (β-$2CaO{\cdot}SiO_2$ (β-C_2S)), periclase (MgO) and fluorite (CaF_2) and trace amounts of free calcium oxide (f-CaO), merwinite ($3CaO{\cdot}MgO{\cdot}2SiO_2$ (C_3MS_2)), and spinel [5].

Over the past decade, the production of AODS in China has continued to grow, with the cumulative output exceeding 18 million tons. At present, the proportion of stainless steel slags that are recycled is low [6], and the portion that is not recycled will inevitably increase the amount of waste to be treated and disposed of in landfills [7]. During storage and disposal, the chromium in AODS requires special attention due to its potential toxicity [8]. Since the late smelting stage of AOD is in a reducing atmosphere, the low oxygen potential inhibits the oxidation of metals and metalloids [9], so that the chromium in the original AODS mainly exists in the metallic and Cr(III)

✉ Ya-nan Zeng
zengyanann@126.com

✉ Jun-guo Li
lijg99@163.com

[1] College of Metallurgy and Energy, North China University of Science and Technology, Tangshan 063210, Hebei, China

[2] School of Metallurgy, Northeastern University, Shenyang 110819, Liaoning, China

states [2]. The chromium oxide in AODS is mainly physically encapsulated in silicate phases or chemically sealed in spinel phases [4]. Cr(III) in the form of Cr_2O_3 has a high activity and can be oxidized to Cr(VI) under alkaline conditions [10]. In the aging process, when AODS absorbs moisture, hydrolysis of the alkaline soluble phase generates $Ca(OH)_2$, making Cr(III) easier to oxidize to Cr(VI). Even at normal temperature, the thermodynamic conditions for the oxidation reaction of chromium can be reached [11]. Cr(VI) has a higher migration capacity and higher toxicity than Cr(III) [12]; therefore, for the long-term stacking of AODS, the change in chromium leaching risk must be considered during disposal and recovery.

In addition to the oxidation reaction, there are also carbonation reactions that will have an important effect on the characteristics of AODS in the long-term aging process. When carbon dioxide and moisture are in contact with the Ca/Mg-containing phases, AODS will be carbonated even under mild aging conditions during the landfill process [13]. Carbonation can significantly change the type, content, and micromorphology of the mineral phases in AODS. The carbonation of AODS mainly consumes the dicalcium silicate phase, and the generated calcium carbonate and silica gel mainly adhere to the surface of the slag particles [14] or fill the areas between the slag particles [15]. The newly generated carbonation products hinder the contact between the soluble mineral phases in the AODS and the external solution and reduce the probability of carbon dioxide penetration into the slag particles. This hinders the further carbonation of the AODS and reduces its ability to release ions [16].

The carbonation reaction consumes the alkaline mineral phases in the AODS, producing carbonates with lower solubility and resulting in a decrease in the alkalinity and metal ion leachabilities of the AODS [17]. Santos et al. [18] found that carbonation can reduce the leachabilities of Mo, Pb, and Zn, but its effect on chromium fluctuates with the carbonation ratio. Fernández Bertos et al. [19] analyzed the cause of the fluctuation in the chromium leachability and pointed out that chromium oxide can replace silicon oxide in C–S–H gel. When the pH of the leachate is moderate, C–S–H gel can dissolve and release chromium. When the pH of the leachate is further reduced, calcium carbonate and the newly formed double salt can absorb chromium again, and thus, its leachability is reduced again.

It should be noted that both oxidation and carbonation can significantly change the mineralogical composition and the presence of chromium. To date, there is still little research on the coupling effect of these two main aging mechanisms. Considering that the AODS piled in stock is still a potentially available resource, it is necessary to study the properties of aged AODS.

This study aims to test the element distribution and mineralogical composition of ten-year-old AODS and analyze how long-term aging influences the chromium leachability. For this purpose, the stratified sampling method was used to collect AODS samples at three positions in a ten-year-old AODS heap. X-ray fluorescence (XRF) spectroscopy analysis was performed to test the chemical components of the three AODS samples. X-ray diffraction (XRD) and scanning electron microscopy (SEM) analyses were performed to study the differences in the phases and microstructures of the slags. Moreover, sequential leaching tests were performed to obtain systematic information on the chromium leachability of the three AODS samples.

2 Experimental

2.1 Sample preparation

The target AODS heap, which was about 15 m in diameter and 7 m in height, had been naturally stacked indoors for one decade and located in the warehouse of a stainless steel production company in China. This batch of AODS was produced at the same time period (within one month) 10 years ago and stored separately as representative waste. Long-term indoor storage prevented the target AODS heap from violent effects such as rainwater leaching and ensured its continuous aging in a relatively stable environment.

Three sets of AODS samples were collected from the surface (S-AODS), middle (M-AODS), and bottom (B-AODS) of the slag heap. The collected samples were crushed and ground and then sieved by a 200-mesh standard sieve. The undersized (< 74 μm) AODSs were placed in a drying oven at 105 °C for 6 h and then stored in a desiccator, ready for all subsequent experiments.

2.2 Characterization

To explore the chemical element distribution evolution of the AODS heap during long-term aging, a test was performed by using XRF analysis on these three sets of AODS samples.

The aging process changed the mineralogical composition of the AODS heap. To obtain comprehensive results for the mineralogical variability within the AODS heap, mineralogical tests were conducted by XRD. The XRD tests were performed on a D8 Advance X-ray diffractometer (Bruker Corporation, Germany), and the diffraction spectra were evaluated in the scanning range of 10° to 90°. The crystalline phases were identified using JADE 9 software based on the ICDD Powder Diffraction File (PDF-2009) database.

The thermogravimetry and differential thermogravimetry (TG–DTG) analysis was used to determine the aged AODS hydration ratio and carbonation degree. TG analysis was conducted using a Setsys Evo TG analyzer (SETARAM, France). Using a cylindrical Al_2O_3 crucible as a sample container, the slag samples were heated from ambient temperature to 950 °C under a nitrogen atmosphere at a heating rate of 0.33 °C/s.

SEM was used to observe the microstructure of the aged AODS samples, and the energy-dispersive spectrometer (EDS) was utilized to obtain the elemental composition information of representative positions in the SEM maps.

2.3 Leaching test

The effect of the aging process on the presence of chromium in AODS could be reflected by the leaching characteristics of chromium. Sequential leaching tests were designed. Using 100 mL of deionized water as the initial leaching solution, 10 g of S-AODS, M-AODS, and B-AODS were taken as the leaching objects. A sealed conical flask was used as the container, and the samples were continuously leached for 20 days in a horizontal shaker at a speed of 20 r/min. In the sequential leaching process, 80 mL of supernatant was sampled every 24 h, and the same amount of deionized water was added to maintain the liquid–solid ratio.

The electrochemical characteristics of the leachate, including pH, redox potential (Eh), and conductivity, are tested immediately after sampling. After filtering through a 0.22-μm membrane filter, chromium ion concentration detection was performed on the sampled leachate. Hexavalent chromium and total chromium concentration in the leachate were analyzed using UV–visible spectrophotometry by the diphenylcarbazide method (GB/T 15555.4–1995) in conjunction with the oxidation of ammonium peroxydisulfate [20]. The trivalent chromium concentration was calculated by the subtraction method.

3 Results and discussion

3.1 Chemical composition

The chemical composition of the unaged original AODS (O-AODS) was recorded in one of our previous studies [21]. Table 1 presents the chemical compositions of the original AODS and the aged AODSs.

Long-term aging did not change the main element composition of the AODS heap. The major components were CaO and SiO_2, which could occupy more than 75% of the total mass. The MgO and Al_2O_3 contents were lower than 10 wt.% and could be classified as minor components, while the TiO_2, Fe_2O_3, MnO, and Cr_2O_3 contents were lower than 1 wt.% and represented trace components.

Regarding the migration of elements in the AODS heap during the aging process, all the elements except magnesium gradually migrated from the surface to the inside. The content of CaO had the largest deviation, which was greater than 8%. It should be noted that the Cr contents in the layers of slag are 0.57, 0.61, and 0.67 wt.%, which could lead to a certain risk of leaching.

3.2 Mineral composition

The XRD analysis results are presented in Fig. 1. The analysis of the different diffraction angles (2θ) and diffraction intensities (I) in the X-ray diffraction spectrum showed that the major mineral components of the S-AODS were dicalcium silicate, merwinite, and pyroxene. Calcite and Fe–Cr spinel were also detected in the XRD spectrum of S-AODS. They could be classified as minor mineral compositions due to the weak intensities of the corresponding diffraction peaks. The mineralogical compositions of the M-AODS and B-AODS were roughly the same as that of S-AODS.

The contents of each mineral contained in each layer of the AOD slag heap were calculated by the adiabatic method by referring to the PDF card provided in the JADE software [22]. The results are listed in Table 2.

The results of the mineral phase quantitative analysis show that after long-term aging, the relative content of the dicalcium silicate phase in the S-AODS was significantly reduced compared to those of the M-AODS and B-AODS, while the content of the calcite was increased. In the process of AODS stacking, the surface slag first contacted CO_2 and H_2O in the air, which formed an environment suitable for carbonation reactions. The generated calcium carbonate and silica gel adhered to the gap between the surface of the AODS and the slag particles [17]. These components played a role in physical encapsulation and hindered the penetration of CO_2 further into the inner part of the slag heap. Thus, these products of S-AODS carbonation protected the internal AODS from being carbonated. In the S-AODS, the dominant phase involved in the carbonation reaction was dicalcium silicate [23]. Therefore, the content of dicalcium silicate in the S-AODS was much lower than those in the M-AODS and B-AODS.

The relative content of the other mineral phases, such as merwinite, pyroxene, and perovskite, did not change much with depth. This may be due to the increase in amorphous products in the slag after the surface slag underwent carbonation, resulting in a change in the relative contents of crystalline substances. It should be noted that the chromium in the surface steel slag mainly existed in the form of iron-chromium spinel, while in the middle and bottom, the

Table 1 Chemical composition distribution of AODS heap (wt.%)

Composition	CaO	SiO_2	MgO	Al_2O_3	TiO_2	Fe_2O_3	MnO	Cr_2O_3
O-AODS	55.90	24.67	5.85	1.07	0.69		0.16	0.51
S-AODS	52.68	23.54	5.63	1.61	0.56	0.48	0.35	0.57
M-AODS	53.42	25.24	5.32	1.95	0.71	0.59	0.31	0.61
B-AODS	61.39	27.59	5.07	1.95	0.99	0.82	0.54	0.67

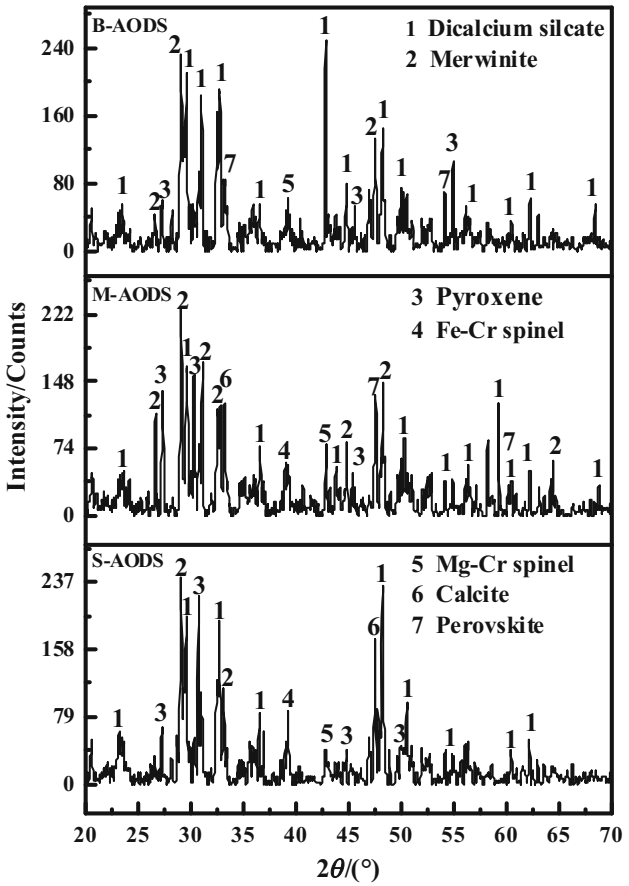

Fig. 1 XRD results for slag samples from AOD stainless steel slag heap

chromium mainly existed in each spinel phase, which may be related to oxidation and rain in the long-term aging process.

3.3 Carbonation degree

The results of the TG-DTG analysis are shown in Fig. 2. It can be seen from the DTG curves that the three slag samples had three obvious characteristic peaks. This indicated that as the temperature increased, there were mainly three mass loss processes for the three aged AODSs. First, the escape of moisture from the interlayer and C–S–H gel occurred in the temperature interval of 100–300 °C [24, 25]. The second mass loss stage detected at temperatures from 400 to 550 °C corresponded to the thermal decomposition of $Ca(OH)_2$ [26]. The third mass loss stage in the temperature range of 550–950 °C corresponded to the thermal decomposition of $CaCO_3$ [27, 28].

From the TG curves of the three slag samples, it can be seen that the calcite decomposition amount of the surface layer is greater than those of the middle layer and the bottom layer. According to the thermogravimetric experimental data, the carbonation degree (CO_2 uptake ratio) of the three slag samples S-AODS, M-AODS, and B-AODS can be calculated according to Eq. (1) as 5.3%, 3.5%, and 1.0%, respectively.

$$w = \frac{\Delta m_{550\rightarrow 950\,^{\circ}\mathrm{C}}}{m_{950\,^{\circ}\mathrm{C}}} \times 100\% \quad (1)$$

Table 2 Mineral contents of each layer of AODS heap (wt.%)

Composition	Dicalcium silicate	Merwinite	Pyroxene	Fe–Cr spinel	Mg–Cr spinel	Calcite	Perovskite
S-AODS	23.95	34.19	25.78	4.77	–	11.31	–
M-AODS	46.92	27.32	26.51	–	6.12	6.97	6.26
B-AODS	48.96	25.01	24.01	–	5.26	3.76	5.35

– indicates trace content

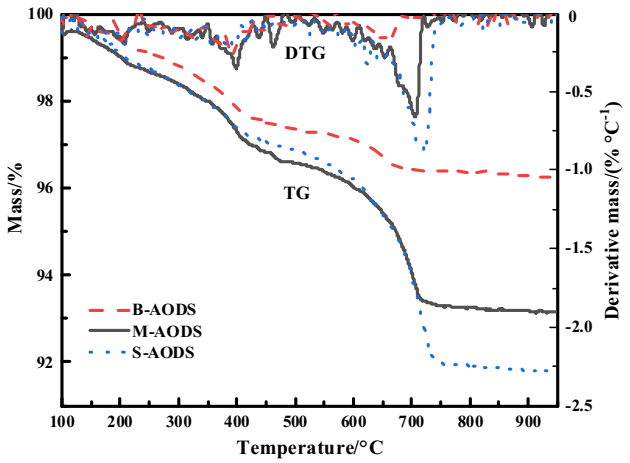

Fig. 2 TG-DTG curves of three sets of AODS

where w denotes the CO_2 uptake ratio; $\Delta m_{550\rightarrow950\,^{\circ}C}$ is the mass loss (decarbonation) from 550 to 950 °C for the aged AODS; and $m_{950\,^{\circ}C}$ is the mass of the aged AODS after dehydration and decarbonation, which is equivalent to the mass of the original AODS.

The results of carbonation degree analysis showed that during the long-term natural aging process, the AODS heap was exposed to air, and indeed, a slow carbonation reaction occurred. Carbonation first started in the S-AODS and gradually penetrated the interior of the slag heap. Products of carbonation, such as calcium carbonate and silica gel, covered the surface of the slag particles or filled the spaces between the slag particles, which hindered further carbonation; therefore, the bottom slag had the lowest degree of carbonation.

3.4 Micromorphology

Figure 3 shows the micromorphology of the S-AODS. The particles of the S-AODS mainly existed in an irregular plate (Fig. 3a, b) or granular form (Fig. 3c, d). Due to the different surface morphologies of the mineral phases present in the slag particles, the number of secondary electrons generated during the SEM imaging process was different, resulting in different shades for the different phases in the photograph. At the positions of phases with different shades, EDS tests were carried out to detect the elemental compositions, and the results are listed in Table 3. According to the SEM and EDS results, the matrix of S-AODS was mainly composed of Ca, Mg, Si, and O, and the mineral phase was mainly C_2S and C_3MS_2. MgO was a minor phase that mainly existed alone in the form of particles. Other trace phases, such as Cr–Mg spinel ($MgO{\cdot}Cr_2O_3$), perovskite ($CaO{\cdot}TiO_2$), and chromium oxide (Cr_2O_3), were mostly encapsulated in these matrix phases.

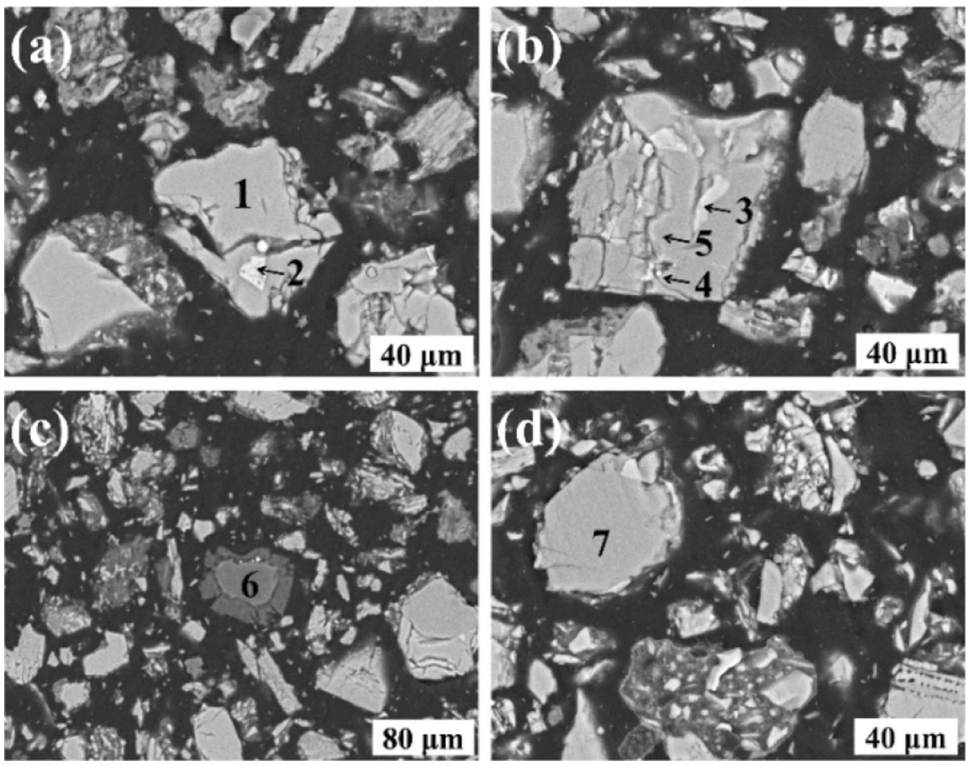

Fig. 3 Micromorphology of S-AODS

Table 3 Element compositions of representative microdomains in S-AODS (at.%)

Microdomain	Ca	Si	Mg	C	O	Cr	Fe	Ti
1	35.60	13.45	–	–	50.95	–	–	–
2	–	–	9.19	19.78	49.53	21.50	–	–
3	24.04	2.84	–	–	54.80	2.41	–	15.92
4	12.69	6.47	–	–	39.30	8.94	32.59	–
5	21.39	10.64	6.94	15.19	45.84	–	–	–
6	–	–	54.21	–	45.79	–	–	–
7	26.93	12.99	8.05	–	52.02	–	–	–
8	35.60	13.45	–	–	50.95	–	–	–

– indicates trace content

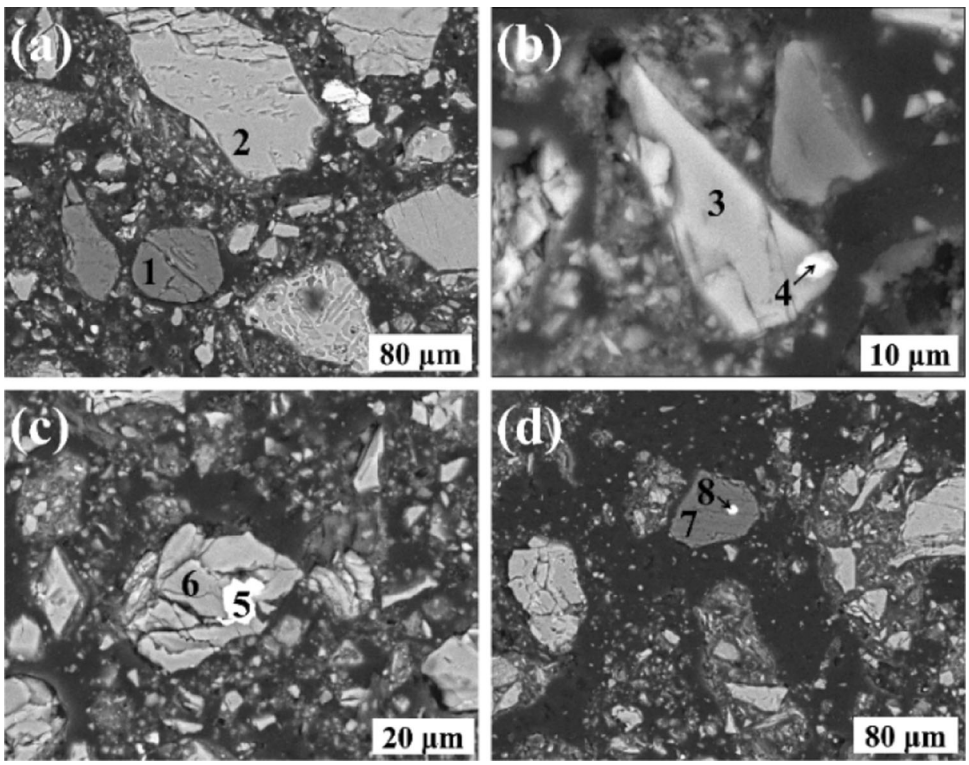

Fig. 4 Micromorphology of M-AODS

Figure 4 shows the micromorphology of the M-AODS. The slag particles of the M-AODS were mostly plate-shaped, circular, elliptical, or irregular. The EDS results listed in Table 4 show that the M-AODS was mainly composed of Ca, Si, Mg, Fe, Cr, and O. In Fig. 4, microdomains 1 and 7 were periclase phases, which existed as separate particles. Microdomain 8 was metallic iron (Fe), which was wrapped in the periclase phase. Similar to the S-AODS, C_2S (Microdomains 2 and 3) and C_3MS_2 (Microdomain 6) existed as the major matrix phases in the M-AODS particles, and trace phases, such as ferrochrome, Fe–Cr spinel, and metal iron, were wrapped by these predominant phases.

Figure 5 and Table 5 show the micromorphology and microdomain element composition of the B-AODS, respectively. The B-AODS was similar to the M-AODS in terms of morphology and phase composition. The slag particles of the B-AODS were mostly circular or irregular plates. The matrix phases (C_2S and C_3MS_2) encapsulated the trace phases (perovskite, ferrochrome, Fe–Cr spinel, and Cr_2O_3), while the minor phase, periclase, existed as individual round particles.

Table 4 Element compositions of representative microdomains in M-AODS (at.%)

Microdomain	Ca	Si	Mg	C	O	Cr	Fe
1	Ca	–	53.66	–	46.34	–	–
2	–	13.40	–	–	50.83	–	–
3	35.77	13.02	–	–	52.58	–	–
4	34.40	–	39.40		51.24	9.36	–
5	–	–	–	–	–	4.96	95.04
6	–	12.96	8.35	–	51.50	–	–
7	27.18	–	53.14	–	46.86	–	–
8	–	–	–	–	–	–	100

– indicates trace content

3.5 Leaching characteristics

As the most important electrochemical indexes of the leachate, the Eh and pH jointly determine the presence of metal ions, which has a great influence on the leachability of the metal ions in the experimental target [29].

Figure 6 shows the evolution characteristics of the pH and Eh of the leachates during the sequential leaching test. First, the leaching time was used as the variable for analysis. During the 20-d sequential leaching, the pH of the leachates of the three AODSs gradually decreased, while the Eh gradually increased. The high alkalinity of the leachate in the initial leaching stage was due to the rapid release of a large amount of hydroxide from the soluble primary phases in the AODSs. As the leaching continued, the single-day hydrolysis rate of the primary phases gradually decreased, thereby reducing the hydroxide release rate. In addition, the formation of the secondary precipitation phase might consume a certain amount of hydroxide, resulting in a gradual decrease in the pH of the leachates. Second, if the distribution position of the slag samples in the slag heap was used as the variable for analysis, as the depth increased, the pH of the leachates gradually increased. This was because the surface slag had undergone carbonation and alkali metal elemental sedimentation during the long-term aging process.

The Eh of the leachates was determined by the pH and the dissolved oxygen (DO) contents [30]. The leaching experiment was carried out in a closed flask that could prevent the oxygen in the environment from entering the leaching system. After the daily sampling, water with the same dissolved oxygen content was added to the flask as a supplementary solution. Therefore, during the leaching process, the DO in the leachates was almost constant, and the pH became the only factor affecting Eh in this study.

The conductivity of the leaching solution can reflect the sum of the ability of the AOD slag to release ions during the leaching process [31]. As shown in Fig. 7, the B-AODS had the highest conductivity during the entire leaching

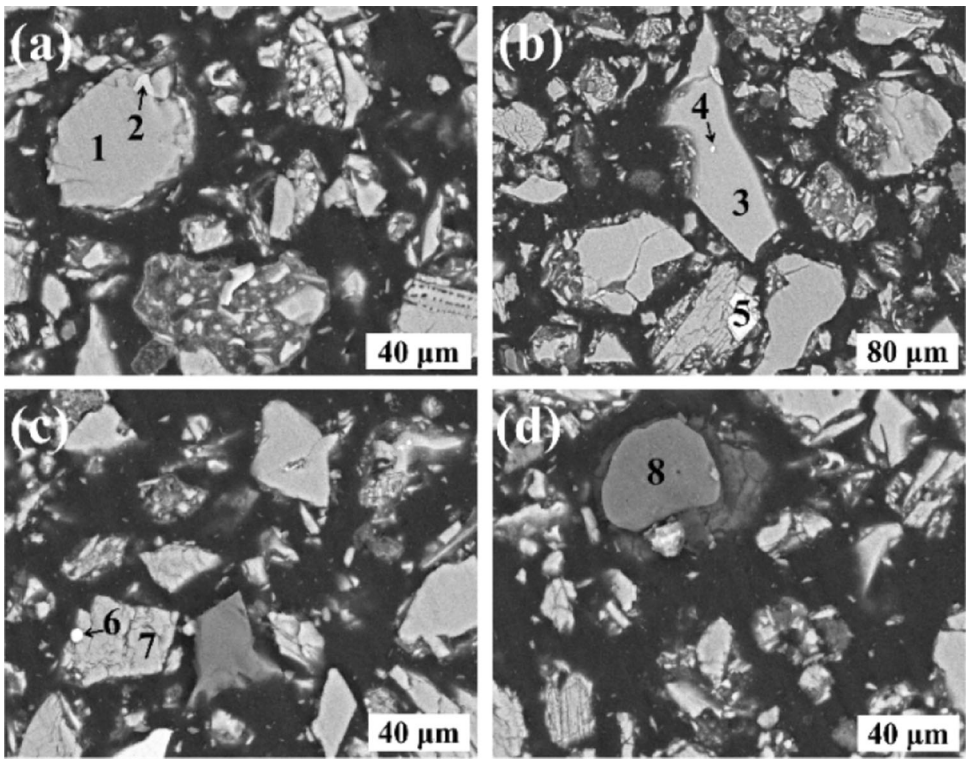

Fig. 5 Micromorphology of B-AODS

Table 5 Element compositions of representative microdomains in B-AODS (at.%)

Microdomain	Ca	Si	Mg	C	O	Cr	Fe	Ti
1	26.93	12.99	8.05	–	52.02	–	–	–
2	22.61	4.18	–	–	58.87	2.22	–	12.12
3	39.40	13.66	–	–	46.94	–	–	–
4	–	–	–	–	–	15.86	84.14	–
5	–	–	–	–	41.48	2.19	56.34	–
6	–	–	–	–	–	20.55	79.45	–
7	35.13	12.93	–	–	51.94	–	–	–
8	–	–	55.79		44.21	–	–	–

– indicates trace content

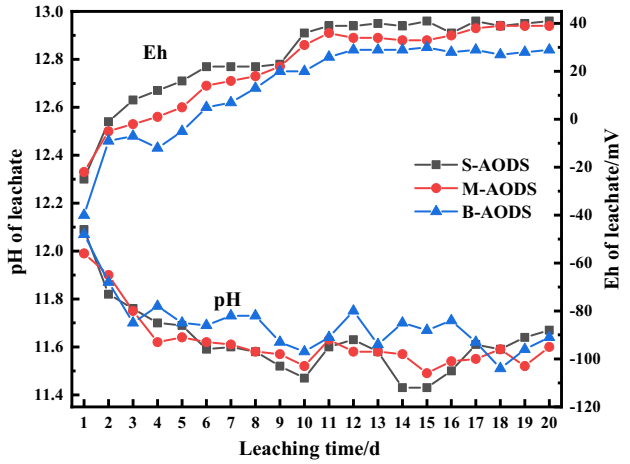

Fig. 6 pH and Eh evolution curves of leachates corresponding to three AODSs

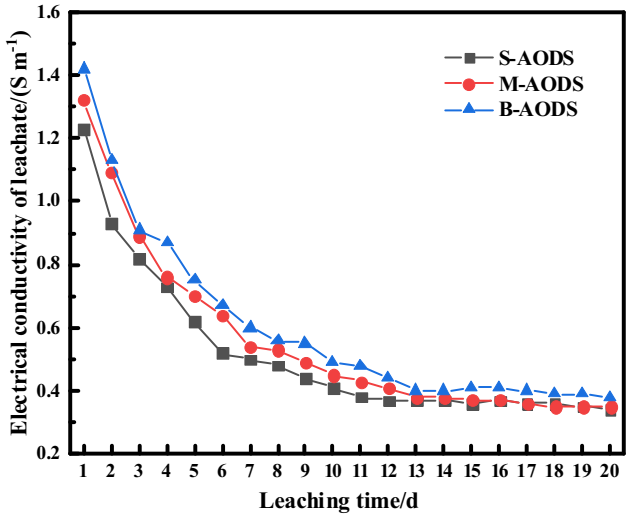

Fig. 7 Conductivity evolution curves of leachates corresponding to three AODS samples

cycle and had the strongest ion leachability, while the S-AODS had the lowest conductivity and the weakest ion leachability.

In the long-term aging process, the S-AODS first contacted the external environment. The oxidation reaction and the carbonation reaction were carried out first in the S-AODS. The soluble elements in the S-AODS slowly migrated to the bottom layer under the action of microleaching and gravity. As shown in the XRF analysis results, Mg was relatively special. According to the SEM/EDS results, Mg existed as a single periclase particle in the AODS and was insoluble in water, so it did not easily migrate. After the chromium was oxidized to hexavalent chromium, its migration ability was greatly increased [32], and it gradually migrated to the bottom layer. The surface slag had also undergone carbonation, which consumed the soluble silicate phases and produced carbonate phases that were much less soluble than these phases, which is an important reason why the S-AODS leachate had the lowest conductivity.

Figure 8a shows that the B-AODS had the strongest chromium leachability, which was significantly higher than those of the M-AODS and the B-AODS. With the extension of the leaching time, the total chromium leached in a single day gradually decreased and tended to leach at a rate of 0.44 mg/(kg d) after the 15th day. Figure 8b shows that during the entire leaching procedure, hexavalent chromium contributed the vast majority of the total chromium leaching amount and showed continuous leachability. In the early stage of leaching, the amount of hexavalent chromium accounted for more than 60% of the total chromium. With the extension of the leaching time, the proportion of hexavalent chromium gradually increased and reached 100% on the 13th day. Regarding the leaching of hexavalent chromium itself, it can be seen from Fig. 8b that the B-AODS had the highest hexavalent chromium leachability, while S-AODS and M-AODS had very similar hexavalent chromium leaching curves.

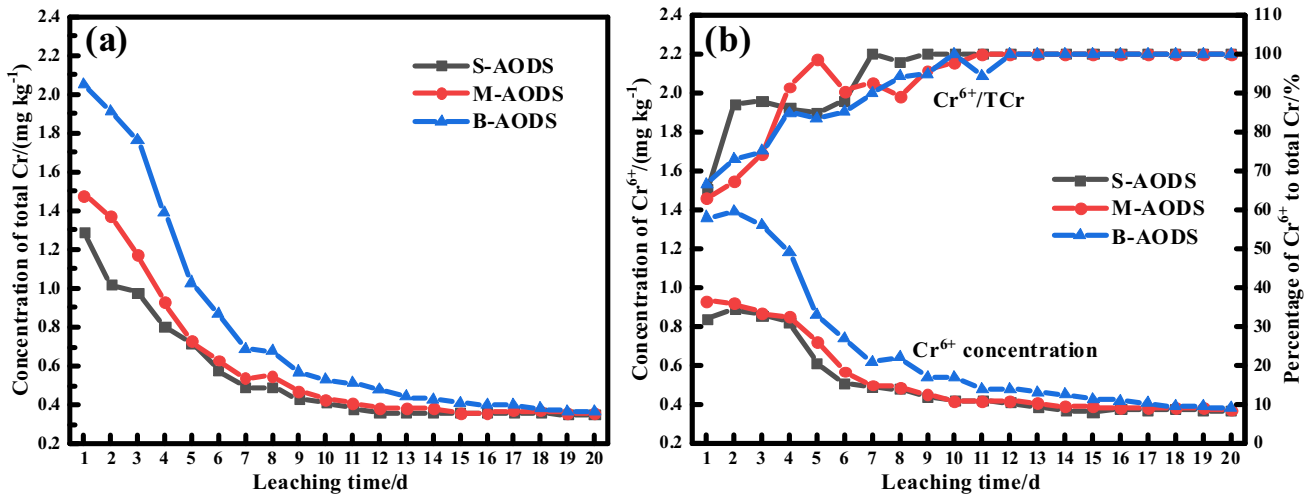

Fig. 8 Total chromium (TCr) (**a**) and hexavalent chromium (**b**) leaching evolution curves for three AODS samples

Due to the reducing smelting environment of the AOD process, the chromium in the original AODS mainly existed in the form of trivalent chromium. After long-term aging, the trivalent chromium was oxidized into hexavalent chromium by oxygen in the air. The hexavalent chromium had higher mobility than the trivalent chromium. Under the combined effect of trace leaching and gravity in the aging environment, more hexavalent chromium was enriched in the B-AODS. The SEM/EDS analysis showed that a large part of the chromium in the aged AODSs existed in the spinel phases (Fe–Cr spinel and Mg–Cr spinel) with strong chemical stability, which occurred because the chromium in the original slag already existed in this state [33, 34]. These Cr-bearing spinel phases cannot be carbonated or oxidized in the natural environment. The growth of hexavalent chromium during the long-term aging process occurred because of the oxidation of the Cr_2O_3 encapsulated in the Ca–Mg–Si matrix phases. This part of the chromium was the main source of chromium released during the leaching process. The proportions of hexavalent chromium of the aged slags and the original slag were different, which affected the leachability of the total chromium.

The aged AODS sample, especially the B-AODS, had high chromium leachability, and there was a certain risk of chromium leaching. Therefore, when handling or recycling these types of solid waste, the potential impact on the environment must be considered.

4 Conclusions

1. The main elements in the AODS, except for magnesium, experienced migration from the surface layer to the bottom layer during the long-term aging process. The content of chromium in the B-AODS was 17.5% higher than that in the S-AODS.
2. During the long-term aging process, the types of mineral phases in the AODS did not change, and calcite formed by carbonation existed in the S-AODS. Dicalcium silicate and merwinite were the dominant mineral phases in the matrix. Chromium was mainly encapsulated in these matrix phases in the form of oxides, alloys, and spinels. Periclase existed as individual particles.
3. Long-term aging had a significant effect on the leachability of the chromium in the AODS. The B-AODS had the highest chromium leachability, which was significantly higher than those of the other two slags. The chromium leachability of the M-AODS was slightly higher than that of the S-AODS.
4. In the aged AODS samples, hexavalent chromium had long-term continuous leachability, while trivalent chromium was not detected after the 13th day of leaching.

Acknowledgements All the authors acknowledge the support of this study by the National Natural Science Foundation of China (Nos. 51704119 and 51574108) and the Key Research and Development Project of Tangshan (No. 19140205F).

References

[1] Stainless Steel Council of China Special Steel Enterprises Association, China's stainless steel crude steel production increased by about 10% to 29.4 million tons in 2019 (Accessed: 2020–03–03). http://www.cssc.org.cn/page137?article_id=2504.
[2] H. Shen, E. Forssberg, U. Nordström, Resour. Conserv. Recy. 40 (2004) 245–271.
[3] R.I. Iacobescu, G.N. Angelopoulos, P.T. Jones, B. Blanpain, Y. Pontikes, J. Clean. Prod. 112 (2016) 872–881.

[4] G. Adegoloye, A.L. Beaucour, S. Ortola, A. Noumowé, Constr. Build. Mater. 76 (2015) 313–321.
[5] S. Zhang, Y. Zhang, Z. Qu, J. Alloy. Compd. 805 (2019) 1106–1116.
[6] X. Wang, D. Geysen, T. Van Gerven, P.T. Jones, B. Blanpain, M. Guo, Front. Chem. Sci. Eng. 11 (2017) 353–362.
[7] Q. Zhao, C. Liu, L. Cao, X. Zheng, M. Jiang, Minerals 8 (2018) 445.
[8] B. Liu, J. Li, Y. Zeng, Z. Wang, Chemosphere 144 (2016) 2052–2057.
[9] P. Chaurand, J. Rose, J. Domas, J.Y. Bottero, J. Geochem. Explor. 88 (2006) 10–14.
[10] N. Sano, in: Proceedings: The Tenth International Ferroalloys Congress, South African Institute of Mining and Metallurgy, Cape Town, South Africa, 2004, pp. 670–677.
[11] H. Kilau, I. Shah, in: L.P. Jackson, A.R. Rohlik, R.A. Conway (Eds.), Hazardous and Industrial Waste Management and Testing: Third Symposium, American Society for Testing and Materials, Philadelphia, USA, 1984, pp. 61–80.
[12] X. Tian, W. Wang, N. Tian, C. Zhou, C. Yang, S. Komarneni, J. Hazard. Mater. 309 (2016) 151–156.
[13] R. Baciocchi, G. Costa, E. Di Bartolomeo, A. Polettini, R. Pomi, Waste. Biomass. Valori. 1 (2010) 467–477.
[14] F. Engström, M.L. Larsson, C. Samuelsson, Å. Sandström, R. Robinson, B. Björkman, Steel. Res. Int. 85 (2014) 607–615.
[15] M.A. Boone, P. Nielsen, T. De Kock, M.N. Boone, M. Quaghebeur, V. Cnudde, Environ. Sci. Technol. 48 (2014) 674–680.
[16] P. Jin, R. Wang, Y. Su, H. Dong, Q. Wang, Constr. Build. Mater. 228 (2019) 117110.
[17] Y.J. Wang, Y.N. Zeng, J.G. Li, Y.Z. Zhang, Y.J. Zhang, Q.Z. Zhao, J. Clean. Prod. 256 (2020) 120377.
[18] R.M. Santos, J. Van Bouwel, E. Vandevelde, G. Mertens, J. Elsen, T. Van Gerven, Int. J. Greenh. Gas Control 17 (2013) 32–45.
[19] M. Fernández Bertos, S.J.R. Simons, C.D. Hills, P.J. Carey, J. Hazard. Mater. 112 (2004) 193–205.
[20] Y.L. Bian, Environ. Sci. Manag. 32 (2007) No. 12, 146–147.
[21] Y.J. Wang, J.G. Li, N. Zheng, Iron Steel Vanadium Titanium 34 (2013) No. 4, 68–72.
[22] Z.M. Wang, J.G. Li, B. Liu, Y.N. Zeng, Z.Y. Gao, Metall. Anal. 37 (2017) No. 1, 15–20.
[23] M. Salman, Ö. Cizer, Y. Pontikes, R.M. Santos, R. Snellings, L. Vandewalle, B. Blanpain, K. Van Balen, Chem. Eng. J. 246 (2014) 39–52.
[24] J. Chang, Y. Fang, X. Shang, Mater. Struct. 49 (2016) 4417–4424.
[25] N. Zhang, H. Li, Y. Zhao, X. Liu, J. Hazard. Mater. 306 (2016) 67–76.
[26] S. Kumar, A. Bandopadhyay, T.C. Alex, R. Kumar, Ceram. Int. 32 (2006) 555–560.
[27] L. Wang, L. Chen, D.C.W. Tsang, J.S. Li, T.L.Y. Yeung, S. Ding, C.S. Poon, Sci. Total Environ. 631–632 (2018) 1321–1327.
[28] Y. Jeong, W.S. Yum, J. Moon, J.E. Oh, J. Clean. Prod. 166 (2017) 649–659.
[29] E. Kim, J. Spooren, K. Broos, P. Nielsen, L. Horckmans, R. Geurts, K.C. Vrancken, M. Quaghebeur, J. Clean. Prod. 117 (2016) 221–228.
[30] H.C. Xu, X.J. Xu, K. Wang, J.G. Huang, J. Univ. Sci. Technol. Suzhou Eng. Technol. 20 (2007) No. 2, 63–66.
[31] Y.L. Chen, M.S. Ko, Y.C. Lai, J.E. Chang, Waste Manage. 31 (2011) 1357–1363.
[32] Z. Stepniewska, A. Wolińska, W. Pióro, Pol. J. Soil Sci. 40 (2007) 139–145.
[33] L. Cao, C. Liu, Q. Zhao, M. Jiang, Metall. Res. Technol. 115 (2018) 114.
[34] Y. Sakai, Y. Yabe, M. Takahashi, A. Iizuka, E. Shibata, T. Nakamura, Ind. Eng. Chem. Res. 52 (2013) 3903–3909.